Three-Dimensional Damage Evolution Measurement in EB-PVD TBCs Using Synchrotron Laminography

Vincent Maurel, Lukas Helfen, Romain Soulignac, Thilo F. Morgeneyer, Alain Koster & Luc Rémy

Oxidation of Metals

ISSN 0030-770X
Volume 79
Combined 3-4

Oxid Met (2013) 79:313-323
DOI 10.1007/s11085-012-9333-3

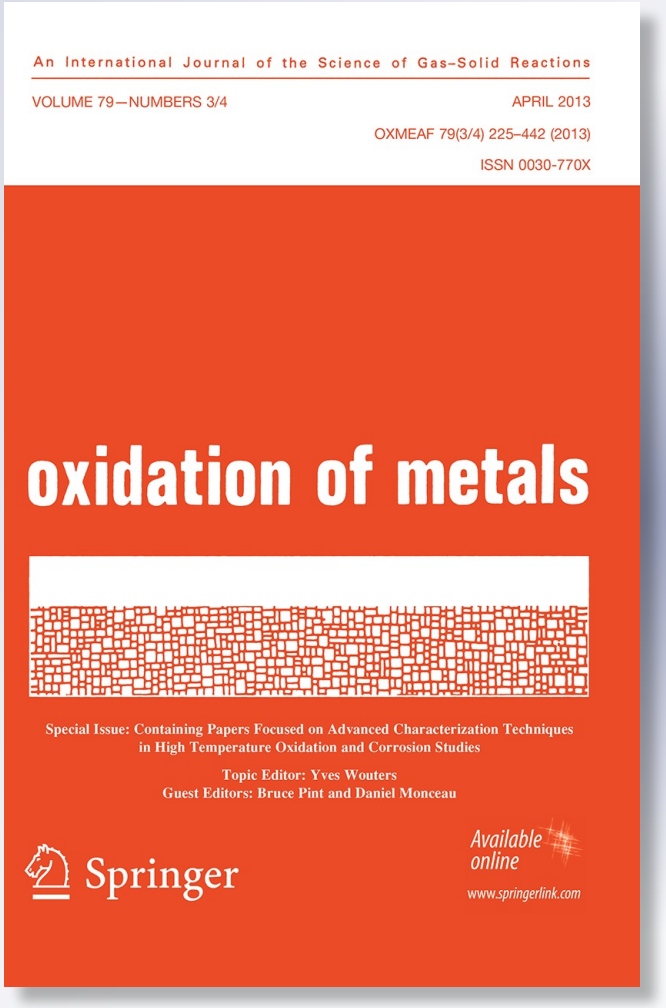

Springer

Oxid Met (2013) 79:313–323
DOI 10.1007/s11085-012-9333-3

ORIGINAL PAPER

Three-Dimensional Damage Evolution Measurement in EB-PVD TBCs Using Synchrotron Laminography

Vincent Maurel · Lukas Helfen · Romain Soulignac · Thilo F. Morgeneyer · Alain Koster · Luc Rémy

Received: 16 April 2012 / Published online: 24 December 2012

Abstract This study provides the first results of three dimensional microstructural evolution analysis of a typical EB-PVD thermal barrier coating subjected to thermal cycling. Results have been obtained using the technique of synchrotron-radiation computed laminography (SRCL), enabling the scanning of samples that are thin but extended in two dimensions. A correlation with quantitative measurements of phase transformation from β-NiAl to γ'-Ni_3Al was achieved from 3D images and 2D cross-section analysis. Morphological features of phase transformation and damaged areas within the bond-coat layer obtained by SRCL are discussed.

V. Maurel (✉) · R. Soulignac · T. F. Morgeneyer · A. Koster · L. Rémy
Centre des Matériaux, Mines ParisTech, UMR CNRS 7633, BP 87, 91003 Evry Cedex, France
e-mail: vincent.maurel@mines-paristech.fr

R. Soulignac
e-mail: romain.soulignac@mines-paristech.fr

T. F. Morgeneyer
e-mail: thilo.morgeneyer@mines-paristech.fr

A. Koster
e-mail: alain.koster@mines-paristech.fr

L. Rémy
e-mail: luc.remy@mines-paristech.fr

L. Helfen
Institute for Photon Science and Synchrotron Radiation (ISS/ANKA), Karlsruhe Institute of Technology, PO Box 3640, 76021 Karlsruhe, Germany
e-mail: lukas.helfen@kit.edu

L. Helfen
European Synchrotron Radiation Facility (ESRF), 6 rue Jules Horowitz, BP 220, 38043 Grenoble, France

R. Soulignac
SNECMA/SAFRAN Group YQMM, Rond point René Ravaud, 77500 Moissy-Cramayel, France

Keywords EB-PVD · Synchrotron computed laminography · Thermal cycling · 3D morphology of Ni_3Al

Issues with 3D Damage Measurement in TBCs

Thermal barrier coatings (TBCs) are often used for thermal insulation and as a passivation system for hot components in industrial applications. TBCs are multilayered systems where interfacial damage can occur preceding ceramic breakaway. This last step is critical since it leads to the loss of substrate protection and damage of the component at high temperatures [1–3].

Thus, measurements of the TBC microstructure and the observation of its evolution under thermal loading is a key point for life assessment and understanding of the damage mechanisms leading to ceramic layer spallation. Moreover, the three dimensional microstructure morphology is known to have an effect on local stress and strain fields resulting in interfacial delamination. Unfortunately, most of the classical metallography specimen preparation techniques could introduce artefacts in the microstructure and confuse subsequent observations. After a long-time exposure of the TBC system at high temperatures, interfacial cracks as well as ceramic layer spallation might even be induced by these preparation techniques with few means being available to determine the true cause of damage. In principle, synchrotron-radiation computed tomography (SRCT) [4] could offer an interesting way of determining the cause of debonding. This technique is very attractive for 3D analysis of the microstructure for an increasing variety of materials [4]. However, SRCT requires samples of small diameter in order to ensure X-ray transmission through the entire volume for all angular projection directions. This point is particularly critical when using strongly absorbing materials like Ni-based superalloys for the coated substrate. It would also complicate the machining of the sample without inducing damage. To address these problems, the technique of synchrotron-radiation computed laminography (SRCL) [5, 6] was developed to scan samples that are still thin but extended in 2 dimensions (such as microelectronic devices [7]). The use of synchrotron radiation is beneficial to laminographic imaging due to the increased spatial resolution achievable compared to established laboratory methods, and due to various highly sensitive phase-contrast modes available based on propagation of the X-ray beam [8, 9] or on wavefront sensing via a grating interferometer [10, 11]. For these reasons, the method has found increased interest also in materials research [8, 9, 12].

A first analysis has shown the potential of investigating EB-PVD thermal barrier coatings via SRCL [13]. It has provided 3D images of the cup-cone structure of the ceramic layer, characterisation of the polycrystalline microstructure of the bond-coat layer and 3D reconstruction of grains and of the interface morphology. Nevertheless, the specimen studied was in the as-processed condition, limiting the contrast between the microstructural features [13].

The aim of this study is to report the first results of the 3D characterisation of electron beam-physical vapour deposition (EB-PVD) TBCs by SRCL after thermal cycling testing.

Experimental Procedures

The Synchrotron-Radiation Computed Laminography (SRCL) Technique

SRCL can be understood as a generalisation of SRCT in which the sample is imaged whilst being rotated around an axis which is inclined by a defined angle θ with respect to the transmitted beam (where θ is 90° for SRCT), see Fig. 1. For planar samples this ensures that the integral X-ray transmission is relatively constant for the different angular projections. This allows large samples to be imaged locally achieving a high resolution [14] without the need for samples containing the regions of interest (ROIs) being physically extracted. The technique has advantages over (limited-angle) SRCT especially when the angular range is restricted [15]. Details about the principles and the reconstruction procedure can be found in Refs [6, 16]. Imaging was performed at beam line ID19 of the ESRF using a polychromatic X-ray beam with energies between approximately 30 and 65 keV. Radiographs with 100 ms exposure time were acquired over a specimen rotation angle of 360° for an axis inclination of θ = 65°. Three dimensional volume images were reconstructed using an in-house software package from 1,500 of such angularly equidistant projection radiographs. The size of the volume analysed was 2,040 × 2,040 × 900 voxels with a voxel size of 0.7^3 μm^3. The ROI was centred in the coupon, leading to a minimum distance between the edge of the coupon and the edge of the ROI of 1.5 mm.

Material and Specimens

The TBC system used in this study was processed by the Ceramic Coating Centre (CCC) and the Snecma–Safran Group. The substrate material was a Ni-based single-crystal superalloy AM1, the composition of which is given in Table 1.

The bond-coat was a Pt-enriched aluminide overlayer (Ni, Pt)Al deposited by pack-cementation. The outer layer was mostly composed of beta phase NiAl, the composition is described in Table 2, and is referred to in the following as the bond-coat (BC) layer. The location of the BC was determined using the line of embedded grit particles, delimiting the inter-diffusion zone (IDZ) between the BC and the substrate (sub.).

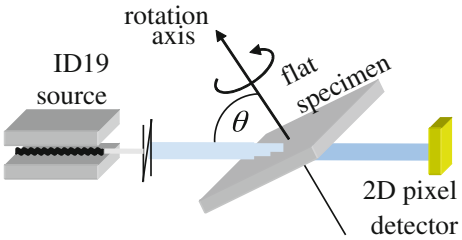

Fig. 1 Experimental set-up sketched for synchrotron-radiation computed laminography (SRCL) with a polychromatic beam at ESRF beamline ID19. The limiting case of θ is 90° corresponds to synchrotron-radiation computed tomography (SRCT) [6]

Table 1 Composition of AM1 (wt%) [17]

	Co	Cr	Mo	W	Ta	Al	Ti	C	Fe	S	Ni
Min	6	7	1.8	5	7.5	5.1	1				Bal.
Max	7	8	2.2	6	8.5	5.5	1.4	0.01	0.2	0.2 ppm	Bal.

Table 2 Initial composition of the β-NiAl Bond Coat (at%) [18]

Co	Cr	Mo	W	Ta	Al	Ti	Ni	Pt
4.6	1	0	0	1	35.2	0	42	7.3

The ceramic layer was an EB-PVD Y_2O_3 partially stabilized zirconia coating 140 µm thick. The TBC system was characterised in its as-received condition by scanning electron microscopy (SEM), see Fig. 2.

Hollow cylindrical test specimens were used for this study to reduce thermal inertia during heating or cooling. The substrate outer diameter was 11 mm within the gauge length and 1 mm in thickness. Each specimen was first cut into a small cylinder of 2 mm length, see Fig. 3a. Then, it was sliced following the dashed line Fig. 3b to extract the coupon to be examined. The final dimensions of the coupon were 500 µm for the maximum thickness and 2 mm in length. Each cut was achieved using a diamond string saw and no further machining was necessary before SRCL scanning.

Cross-section analysis was performed. The coupons were mounted in thermo-formed resin and polished to a mirror-like finish for SEM analysis, see Fig. 2. Etching was used in order to increase the optical contrast between beta and gamma'

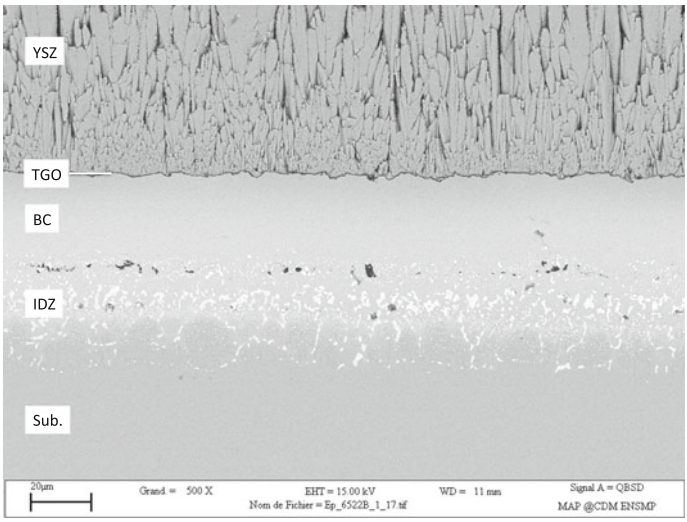

Fig. 2 SEM cross section of the TBC system in the as-received condition

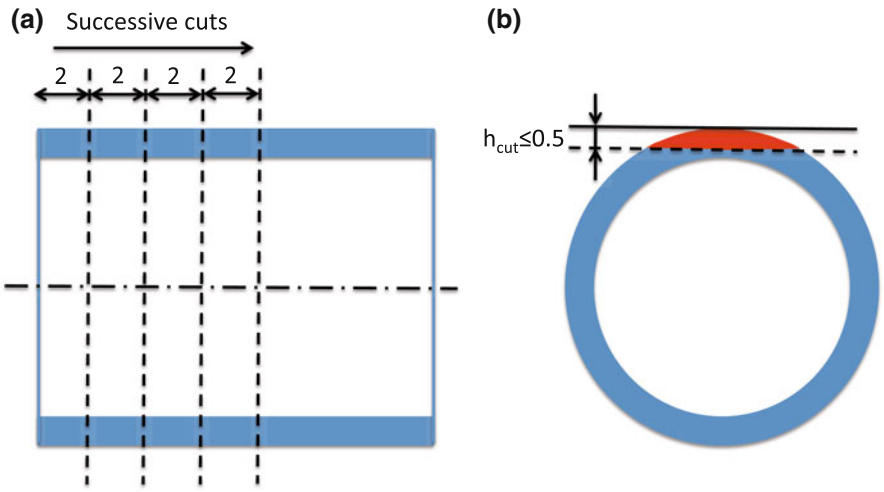

Fig. 3 Sketch of specimen machining, *dashed lines* mark the cutting plane made in the plane orthogonal to the picture. **a** is a cross-section of the initial tubular specimen within the gauge length where first step of cutting is carried out for each interrupted test; **b** is the associated orthogonal view highlighting in *red* the final shape of the coupon obtained for each sliced part from (**a**) (Color figure online)

phases. Large areas were stitched together to increase the reliability of phase transformation measurement using optical microscopy (OM) as a time saving method.

Thermal cycling tests with a dwell time of 5 min at 1,100 °C were performed in air using lamp furnaces. The heating and cooling rates were precisely controlled and set to 5 °C/s within the 100–1,100 °C range. An interrupted test procedure was used to determine the evolution of the TBC microstructure as a function of the number of cycles. Coupons were obtained in the as-received condition and after test interruptions at 75, 200 and 1,200 cycles respectively. The above preparation technique was applied for each coupon.

Cross-Sectional Analysis

SEM was used to study the evolution of the oxide layer during thermal cycling, see Fig. 4a and b. Roughening of the TBC/BC interface can be seen. Small cracks appeared between the ceramic columns and TGO, see the inset of Fig. 4b. Moreover, internal porosity appeared within the oxide at the highest number of testing cycles. However, the observed damage within the oxide layer could have been increased by specimen preparation. No macroscopic ceramic spallation was observed for this last step.

Due to a relatively poor contrast between β-NiAl and γ'-Ni_3Al phases, even in the BSE mode, SEM was complemented by optical microscopy measurements. Employing OM after etching, it was straightforward to increase the contrast between β and γ'-Ni_3Al phases [19], see Fig. 3c and d. γ'-Ni_3Al phase precipitations are seen to initiate in the bulk of the bond-coat and could be assumed to be

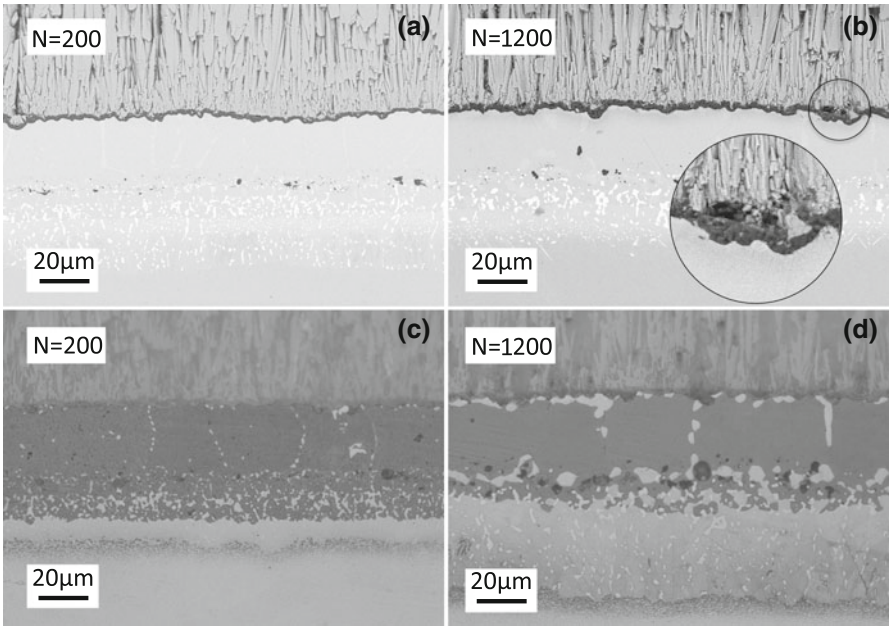

Fig. 4 Cross sections of the TBC system after thermal cycling observed by SEM using BSE, **a** for N = 200 cycles, **b** for N = 1,200 cycles, a *zoom* is inserted; and compared to OM after etching, **c** for N = 200 cycles and **d** for N = 1,200 cycles

preferentially localised on the β-NiAl grain boundaries, see Fig. 4c. Increasing the number of cycles leads to gamma' growth on the β-NiAl grain boundaries, see Fig. 4d. The γ'-Ni_3Al precipitates were seen to be also localised respectively at the BC/IDZ and TGO/BC interfaces, see Fig. 4d. This result is consistent with observations made previously [2, 20].

TBC Microstructure Measurement Using Synchrotron-Radiation Computed Laminography (SRCL)

Laminography Observations

A representative reconstructed 3D view of SRCL data of the specimen is shown in Fig. 5. This image was obtained without filtering. Ceramic columns can be clearly seen, as well as porosity localised at the BC/IDZ interface. At the ceramic/BC interface, gamma' precipitates appear in white as well as in the bulk of the BC.

To obtain information on the evolution of the microstructure, emphasis will be focused in the following on the BC layer and the transition area between BC and ceramic columns.

Cross sections within the BC layer were extracted from the 3D images of the TBC, see Fig. 6. Noise in the reconstructed images was reduced using a Gaussian blur filter. At the ceramic/BC interface, γ'-Ni_3Al precipitates were seen in bright

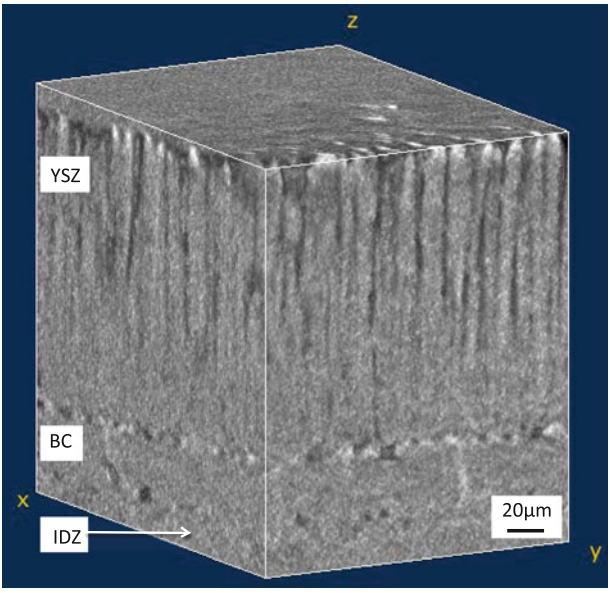

Fig. 5 3D view of the TBC system obtained by SRCL for N = 1,200 cycles

and alternate with interfacial defects in dark, see right of the (yz) cut and at the bottom of the (xz) cut. The γ'-Ni_3Al precipitates, close to the BC/ceramic interface, are consistent in size and location with the 2D SEM cross-section presented in Fig. 4. It is worth noting that in the (xy) plane, γ'-Ni_3Al precipitates could be assumed to be mostly located at triple junction lines of initial β-NiAl grain boundaries.

Based on this observation, 3D images of gamma' precipitates were obtained using a grey level threshold, see Fig. 7a and b.

The top view of the ceramic/BC interface has shown a large spread of γ'-Ni_3Al precipitation, see Fig. 7a. On the other hand, in the bulk of the BC, gamma' precipitation is seen to be mostly localised at triple junction lines, see Fig. 7b obtained with a virtual cut following the dashed line of Fig. 7a.

A similar virtual cross-section is presented in Fig. 8a. This image was obtained without the use of a grey level threshold. Damaged areas appear in dark and γ'-Ni_3Al precipitates appear in bright. Damaged areas are seen to be located within the TGO layer, see Fig. 8a, and are consistent in size and location with observations obtained from cross-sections observed by SEM, see Fig. 4b. These areas could be due to locally thicker oxides, rougher interface as well as interfacial cracks.

Could initial NiAl grain boundaries and NiAl microstructure influence localisation of damaged areas? This point could be discussed observing triple junction lines. Using cross-sections orthogonal to the layer plane, in this case orthogonal to the (xy) plane in Fig. 6, no evidence of this correlation can be seen. This lack of correlation could be related to, firstly, the discontinuity in γ' precipitation along a given triple junction line, see Figs. 4d and 7b. Secondly, the 3D orientation of triple junction lines could inhibit their observation in cross-section. Therefore, Fig. 8b

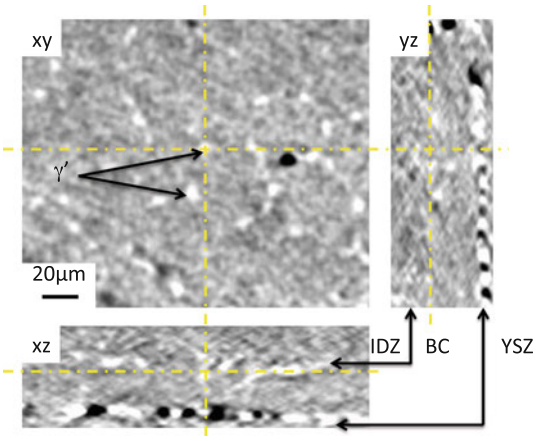

Fig. 6 Mutually perpendicular cross sections obtained by SRCL associated with Fig. 5. The (xy) section corresponds to the external bond-coat layer

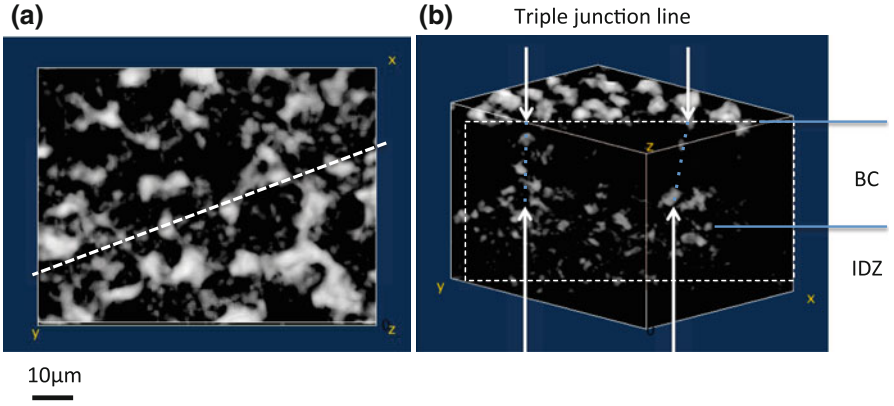

Fig. 7 γ' precipitation obtained by SRCL associated with Fig. 6. *White arrows* indicate the triple junction lines. In **a** the *dashed line* corresponds to the *dashed rectangle* in (**b**), N = 1,200 cycles

was obtained after averaging the thresholded images of γ' precipitates along the z-direction, see white and grey in Fig. 8b. This procedure has enabled the projected location of the triple junction line to be determined, see white points in Fig. 8b. Damaged areas were added onto the obtained picture, see red points in Fig. 8b. This analysis has revealed, that these damaged areas are more or less localised along the grain boundaries of initial NiAl grains observed below the ceramic/BC interface (grain boundaries should be related to γ' location within the BC). Deviation could be related to the 3D orientation of the triple junction line and uncertainty about the exact location of grain boundaries. A quantitative analysis of this correlation between NiAl grain boundaries and damage localisation is under way but is rather complex. Nevertheless this fact was clearly observed in most studied areas of the above set of specimens.

The volume change associated with beta to γ' transformation, proposed by Tolpygo and Clarke [17] as damage mechanism, was shown by Evans [21] to be mitigated by volume changes associated with the oxide growth. It is worth noting

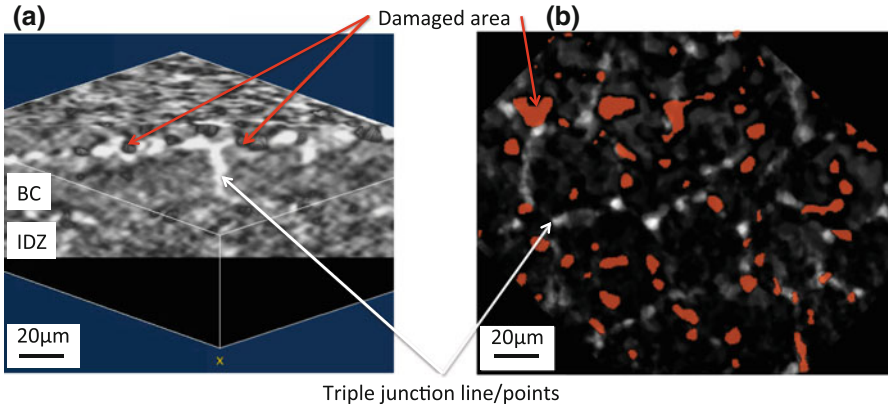

Fig. 8 Virtual cross-section associated to Fig. 6. *White arrows* indicate the triple junction lines and *red arrows* indicate local damaged area, N = 1,200 cycles; **a** perspective view **b** sum over the BC of γ'-Ni_3Al precipitates in white, damaged area in *red* (Color figure online)

that, in our observations, remaining damaged areas were localised above the BC grain bulk. Moreover these areas are located between γ' precipitates close to the ceramic/BC interface. This last point could be related to the assumption proposed by Darzens et al. [22] that the γ' precipitates strength is much higher than the strength of the beta phase. This could trigger a downward motion of the β-NiAl phase during thermal cycling and lead to subsequent remaining cracking located over the bulk of these β-NiAl grains.

Quantitative Comparison of 2D and 3D Measurements

The phase transformation was measured with optical microscopy images performed on cross-section after etching, see Fig. 4c and d. Virtual cross-sections obtained from SRCL measurement were also analysed. Image analysis was performed using the ImageJ software [23]. The brightness and contrast levels were first adjusted to optimise the visualisation of both γ' precipitates and damaged areas. Then, a thresholding technique was used to obtain binary images of both the γ' precipitates and the damaged areas. The same procedure was applied to 2D and 3D images.

The 2D and 3D surface fraction measurement of γ' has provided very similar results, see Fig. 9. This can be considered as a first validation of the quantitative measurements obtained by SRCL.

Moreover, a direct 3D measurement of the γ' volume fraction could be obtained using SRCL images. Once again, the brightness and contrast levels were optimised. The threshold value was the same for 2D and 3D analysis. The volume of locally damaged ceramic/BC areas, due to a locally thick oxide, rough interface or interfacial cracks seems to follow a parabolic law that may be correlated to the average oxide growth [21]. Further analyses are needed, however, to ascertain these latter measurements.

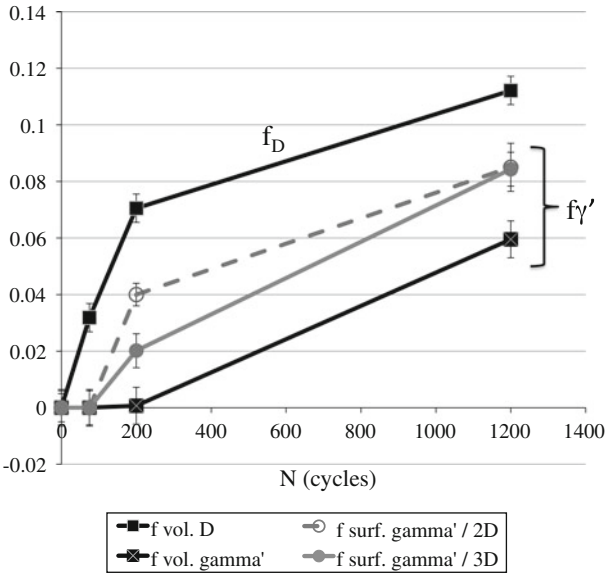

Fig. 9 Evolution of phase transformation from β-NiAl to γ'-Ni_3Al and damage of the ceramic/BC interface. Surface fraction of phase transformation measured by optical microscopy (f surf. gamma' / 2D) were compared with laminography measurements (f surf. gamma' / 3D); gamma' volume fraction (f vol. gamma') as interfacial damage volume fraction (f vol. D) were obtained by laminography

Conclusions

This study has reported the first 3D analysis of EB-PVD microstructure evolution during thermal cycling. The comparison between conventional cross-section measurements and reconstructed 3D images affirms these results. 3D analysis has allowed the link between initial β-NiAl grain microstructure and γ'-Ni_3Al localisation of precipitations to be revealed. γ'-Ni_3Al are mostly located at the TGO/BC and BC/IDZ interfaces and at the triple junction lines of the initial β-NiAl polycrystal. 3D image analysis has also allowed some correlations to be drawn between interfacial damaged areas and the γ' precipitation localisation. Further analyses are underway to compare these results to the effects of various loadings conditions. Moreover, these results could provide the basis for a full 3D mechanical finite element analysis of TBC systems.

Acknowledgments Steve Duvinage and Matthieu Rambaudon (Centre des Matériaux) are gratefully acknowledged for specimen preparation and thermal cycling experiment. Pierre Sallot (Centre des Matériaux/Safran) is also acknowledged for precious advice given for specimen preparation for optical observations.

References

1. P. K. Wright and A. G. Evans, *Current Opinion in Solid State and Materials Science* **4**, (3), 1999 (255).

2. N. Yanar, F. Pettit and G. Meier, *Metallurgical and Materials Transactions A* **37**, (5), 2006 (1563).
3. C. Courcier, V. Maurel, L. Rémy, S. Quilici, I. Rouzou and A. Phelippeau, *Surface and Coatings Technology* **205**, (13–14), 2011 (3763).
4. S. R. Stock, *International Materials Reviews* **53**, (3), 2008 (129).
5. L. Helfen, T. Baumbach, P. Mikulík, D. Kiel, P. Pernot, P. Cloetens and J. Baruchel, *Applied Physics Letters* **86**, 2005 (071915).
6. L. Helfen, A. Myagotin, P. Mikulík, P. Pernot, A. Voropaev, M. Elyyan, M. Di Michiel, J. Baruchel and T. Baumbach, *Review of Science Instruments* **82**, 2011 (063702).
7. L. Helfen, A. Myagotin, A. Rack, P. Pernot, P. Mikulík, M. DiMichiel and T. Baumbach, *Physica Status Solidi (a)* **204**, 2007 (2760).
8. L. Helfen, T. Baumbach, P. Cloetens and J. Baruchel, *Applied Physics Letters* **94**, 2009 (104103).
9. F. Xu, L. Helfen, A. J. Moffat, G. Johnson, I. Sinclair and T. Baumbach, *Journal of Synchrotron Radiation* **17**, 2010 (222).
10. S. Harasse, W. Yashiro and A. Momose, *Optics Express* **19**, 2011 (16560).
11. V. Altapova, L. Helfen, A. Myagotin, D. Hänschke, J. Moosmann, J. Gunneweg and T. Baumbach, *Optics Express* **20**, 2012 (6496).
12. T. F. Morgeneyer, L. Helfen, I. Sinclair, H. Proudhon, F. Xu and T. Baumbach, *Scripta Materialia* **65**, (11), 2011 (1010).
13. V. Maurel, L. Helfen, F. N'Guyen, A. Koster, M. Di Michiel, T. Baumbach and T. F. Morgeneyer, *Scripta Materialia* **66**, (7), 2012 (471).
14. L. Helfen, T. Baumbach, P. Pernot, P. Mikulík, M. DiMichiel and J. Baruchel, *Proceedings of SPIE* **6318**, 2006 (63180N).
15. F. Xu, L. Helfen, T. Baumbach and H. Suhonen, *Optics Express* **20**, 2012 (794).
16. A. Myagotin, A. Voropaev, L. Helfen, D. Hänschke, and T. Baumbach, Fast volume reconstruction for parallel-beam computed laminography by filtered backprojection, manuscript submitted (2012).
17. I. Rouzou, R. Molins, L. Rémy, and F. Jomard. Study of the sulfur segregation for a TBC system. In *High Temperature Corrosion and Protection of Materials 6, Prt 1 and 2, Proceedings* eds. P. Steinmetz, I. G. Wright, G. Meier, A. Galerie, B. Pieraggi and R. Podor, Vol. 461–464 of Materials Science Forum, pp. 101–108, 2004. 6th International Symposium on High Temperature Corrosion and Protection of Materials, Les Embiez, France, May 16–21, 2004.
18. R. Molins, C. Guerre and L. Rémy, *La Revue de Métallurgie-CIT/Science et Génie des Matériaux* **5**, 2003 (507).
19. P. Sallot, V. Maurel, and L. Rémy. Microstructural damage criterion for Ni based single crystal superalloy coated with NiAlPt, 39th International Conference on Metallurgical Coatings and Thin Films (ICMCTF), ICMCTF 2012.
20. V. K. Tolpygo and D. R. Clarke, *Acta Materialia* **48**, 2000 (3283–3293).
21. H. E. Evans, *Surface and Coatings Technology* **206**, (7), 2011 (1512).
22. S. Darzens, D. R. Mumm, D. R. Clarke and A. G. Evans, *Metallurgical and Materials Transactions A: Physical Metallurgy and Materials Science* **34A**, (3), 2003 (511).
23. Image J. Image processing and analysis in java, v1.46 m. http://imagej.nih.gov/ij/, 2012.